Max-Planck-Institut
für Mathematik
in den Naturwissenschaften
Leipzig

Low energy domain patterns in soft ferromagnetic films

by

A. DeSimone, R. V. Kohn, S. Müller, F. Otto and R. Schäfer

Preprint no.: 77 2001

LOW ENERGY DOMAIN PATTERNS IN SOFT FERROMAGNETIC FILMS

A. DESIMONE, R.V. KOHN, S. MÜLLER, F. OTTO AND R. SCHÄFER

Abstract. Computations based on a two-dimensional model recently proposed by the authors shed some new light on classical experimental observations of permalloy films under in-plane applied magnetic fields.

Some quantities, such as the magnetic charge density or the magnetization in the regions of the film where the external field penetrates the sample are easily and robustly computable through energy minimization and are much less prone to hysteresis than the underlying domain structures.

Introduction

Driven by the allure of spin electronics, soft ferromagnetic films are enjoying renewed attention. Most current modelling is based on direct micromagnetic simulation, which is the tool of choice for the study of hysteresis and dynamic switching. It is however natural to try and complement this effort by seeking a more analytical understanding of domain patterns, starting from the study of equilibrium configurations. In this spirit, a two-dimensional variational model has been recently derived from micromagnetics, and used by the authors for the computation of energy minimizing domain patterns in permalloy films with square cross-section subject to an in-plane applied magnetic field [1]. Our results fall in two categories.

The first one concerns the structure of the energy functional of micromagnetics, in the thin-film limit. This limit process reveals a hierarchical structure in the energy, which separates into low-order terms, "essential part", and higher-order terms. The low-order terms lead to constraints (e.g. the component of the magnetization along the thickness direction must vanish), hence to the elimination of degrees of freedom. The essential part is the term of second order in the film thickness: it leads to a (new) reduced variational principle which sets the charge density. Wall energies and anisotropy contribute only at higher order. The higher-order terms are not irrelevant: they provide the energy barriers which are the source of magnetic hysteresis. Moreover, they break the degeneracy in the reduced theory.

The second one concerns the quantitative tools at our disposal to analyze the experimentally observed response of soft ferromagnetic films. There are some quantities, such as the charge density and the magnetization in parts of the sample (the regions of "penetration" of the external field, which grow larger with the strength of the applied field), which are uniquely determined by energetics at leading order. These quantities are easily and robustly computable, and seem to be less prone

Date: October 5, 2001

Accepted for publication in Journal of Magnetism and Magnetic Materials (2002).

Key words and phrases. thin-film-permalloy, domain patterns, hysteresis, micromagnetics.

to hysteresis than the underlying domain patterns. Thus, they may play a significant role in the study of the microstructural origin of magnetic hysteresis in soft ferromagnetic films.

Micromagnetics in the thin-film limit

The free-energy functional of micromagnetics in units of $J_s^2 L^3/2\mu_0$ is

$$\begin{aligned} E_d(m) &= (\kappa d)^2 \int_{\Omega_d} |\nabla m|^2 dx + Q \int_{\Omega_d} \varphi(m) dx \\ &+ \int_{R^3} |h_d|^2 dx - 2 \int_{\Omega_d} h_e' \cdot m dx \,. \end{aligned} \tag{1}$$

Here m is the magnetization (in units of the saturation magnetization J_s), a unit vector field defined on the film Ω_d with cross section ω and thickness d, where all lengths are measured in units of a typical lateral dimension L (the edge-length for ω a square). Moreover, κ is the ratio between exchange length D_{BL} and film thickness, where $D_{BL} = (2\mu_0 A/J_s^2)^{\frac{1}{2}}$, and A is the exchange constant; Q is the quality factor measuring the strength of the magnetic anisotropy φ relative to that of dipolar interactions; h_d is the stray field in units of J_s/μ_0, and the corresponding integral is the magnetostatic energy; h_e' is the applied field in units of J_s/μ_0, which we assume to be uniform and parallel to the film's cross section. In what follows, a prime will always denote a two-dimensional field or operator.

For $d \ll 1$ a hierarchical structure emerges in (1), which is summarized in Table 1. Variations of m of order one along the thickness direction x_3 give rise to an exchange energy per unit area (of the cross section) of order $\kappa^2 d$. An out–of–plane component m_3 of order one determines a magnetostatic contribution per unit area of order d. The component of the in-plane magnetization m' orthogonal to the lateral boundary $\partial\omega$ of the film's cross section ω leads to a magnetostatic contribution of order $d^2 \ln \frac{1}{d}$ per unit length. The same mechanism penalizes jumps $[m' \cdot \nu']$ of the normal component of the magnetization across a line of discontinuity of m' with normal ν'. These lines of discontinuity arise as sharp interface approximations of domain walls. At order d^2 we find the magnetostatic energy per unit area due to surface "charges" proportional to the in-plane divergence $\mathrm{div}' m'$. Finally, the energy per unit length of a Néel or asymmetric Bloch wall and the energy of a single vortex are indicated in the table. In the regime

$$H_e' = \frac{h_e'}{d} \sim 1, \quad \frac{Q}{d} \ll 1, \quad d \ll \kappa^2 \ll \frac{1}{d \ln\left(\frac{1}{d}\right)}\,, \tag{2}$$

the low-order terms penalizing m_3, $\frac{\partial m}{\partial x_3}$ and $[m' \cdot \nu']$ become hard constraints, forcing the corresponding energy sources to vanish, while the energetic cost of anisotropy, of the wall type of minimal energy, and of vortices become higher-order terms. The energy is thus determined, at principal order, by the competition between the aligning effect of H_e' and the demagnetizing effects due to $\mathrm{div}' m'$.

In view of this separation of energy scales in the regime (2), the following reduced theory emerges naturally. The magnetization should be such that $m'(x')$ minimize

$$E(m') = \int_{R^3} |H_d|^2 \, dx - 2 \int_{\omega} H_e' \cdot m' \, dx', \tag{3}$$

where $H_d(x) = -\nabla U$ is determined by

$$\begin{aligned} \nabla^2 U &= 0 \text{ in } R^3 \text{ outside of } \omega, \\ \left[\frac{\partial U}{\partial x_3}\right] &= \mathrm{div}' m' \text{ on } \omega, \end{aligned}$$

among all in-plane vector fields m' of at most unit length

$$|m_0'| \le 1 \text{ in } \omega, \tag{4}$$

which satisfy $[m' \cdot \nu'] = 0$ across all possible discontinuity lines and at $\partial\omega$ (we will call *regular* all magnetizations satisfying this condition).

A rigorous proof justifying our theory beyond the heuristic arguments given above will be published elsewhere. Here, we just remark that (3) extends the models of van den Berg [2] and Bryant and Suhl [3] to arbitrary field strengths, it provides them with a variational formulation, and it clarifies their relationship with micromagnetics.

Computations based on the reduced theory

To bring into focus our proposed algorithm for the computation of low-energy domain patterns, let us first identify the quantities which can be uniquely determined by minimizing (3). The functional E depends on m' only via the surface charge $\sigma = -\mathrm{div}' m'$, and it is not hard to show that E is strictly convex in σ. Thus, energy minimization determines σ uniquely and, through the scalar potential U, it also gives the stray field H_d. The magnetization is instead uniquely determined only in some parts of the sample. To see this, observe that any minimizer m' of (3) satisfies the Euler-Lagrange equation

$$H_d' + H_e' = \lambda\, m' \text{ in } \omega, \tag{5}$$

where $\lambda(x')$ is the Lagrange multiplier associated with the pointwise constraint (4). There exists a finite critical field strength H_{crit}, in the following sense: when the applied field is subcritical, $\lambda \equiv 0$ and the external field is completely expelled from the sample, whereas when it is supercritical λ is nonzero somewhere and the field penetrates in that part of the sample. The critical field strength depends on the geometry of ω — for a circular disk of diameter one, its value is one. Since H_d is uniquely determined, the region $\{H_d' + H_e' \neq 0\}$ of ω where the external field is not expelled from the sample is uniquely determined. Within this penetrated region, m' is also uniquely determined in view of (5), and it is of unit length.

Outside the regions of field penetration, the magnetization is not uniquely detemined by energy minimization. Moreover, the energy (3) is insensitive to requiring that minimizing magnetizations satisfy (4) or rather the unit length constraint

$$|m'| = 1 \text{ in } \omega. \tag{6}$$

In fact, for any regular m_0' of at most unit length there exist many regular m' of unit length with the same surface charge: $\mathrm{div}' m' = \mathrm{div}' m_0'$. Indeed, we may write $m' = \nabla^\perp \psi + m_0'$ where $\nabla^\perp \psi = (-\partial\psi/\partial x_2, \partial\psi/\partial x_1)$ and the continuous function $\psi(x')$ on ω solves the boundary value problem

$$|\nabla^\perp \psi + m_0'| = 1 \text{ in } \omega, \tag{7}$$

$$\psi = 0 \text{ on } \partial\omega. \tag{8}$$

One can generate many solutions of this problem by imposing the additional condition $\psi = 0$ on an arbitrary curve contained in ω.

The considerations above suggest the following two-step scheme for the numerical computation of energy minimizing domain patterns. The first step minimizes (3) among all regular in–plane vector fields m_0' of length *less than or equal to* 1. This step is used to identify all quantities that are uniquely predicted by energy minimization (in particular, the region of field penetration and the magnetization within this region). Note, however, that m_0' typically violates (6) outside the region of field penetration. Here, the unit length constraint is restored in the second step, which postprocesses m_0' by solving (7,8) to obtain another minimizer m' which also satisfies (6). This m' is used to identify a low energy domain pattern.

The first step is a convex variational problem. We solve it by using an interior point method [4]. For the second step, we recall that the solution of (7,8) is not unique. What we compute is a special solution ψ, known as the "viscosity solution", which has special mathematical properties [5], and which can be computed efficiently using the "level set method" [6]. The selection principle implicit in this scheme appears to pick a minimizer with as few walls as possible. The more physical selection mechanism of minimizing wall energy will require to incorporate higher-order corrections in the model.

Experiments as seen by the reduced theory

We have observed the response of two ac-demagnetized Permalloy ($Ni_{81}Fe_{19}$, $J_s = 1.0$ T) square samples of edge lengths $L = 30$ and 60 μm and thicknesses $D = 40$ and 230 nm, respectively, in a digitally enhanced Kerr microscope. Starting from the configuration of Fig. 1, a field applied along the diagonal, and pointing towards the upper right corner, will push the central vortex towards the upper left corner.

The reduced theory seems to capture remarkably well the behavior observed under monotonically increasing fields, both for the thin samples and for the thick ones (these are the ones shown in Fig. 2). The most conspicuous difference in the behavior exhibited by the two types of samples is in their hysteretic response. For the thinner samples, the behavior is reversible upon subsequent reduction of the field, at least up to the maximum field strength $H \cong 1.5$ we applied. Here

$$H = \frac{L}{D}\frac{h_e}{J_s}. \tag{9}$$

and h_e is measured in Tesla. In the thicker samples, the onset of hysteretic behavior is well below $H = 1$.

From the point of view of domain patterns, there are two critical events which seem to be related to the irreversibility exhibited by the thicker samples. The first one is the expulsion of parts of the domain walls from the interior of the sample. Our computations show that this phenomenon is related to the penetration of the external field, see Fig. 3, where we have superimposed on each gray-scale plot (of the vertical component of the magnetization) the level curves of the potential v of the penetrated field, defined by $-\nabla v = H_d' + H_e'$. Regions where the field lines concentrate are regions where $\nabla v \neq 0$, i.e., where the external field has penetrated the sample. Within them, (5) implies that m' is parallel to ∇v, i.e., the magnetization vector is orthogonal to the circular arcs shown in the figures.

At higher fields, the vortex is expelled from the upper left corner, and the more symmetric configuration of Fig. 4 is reached. Our computations show that, at these

TABLE 1. Scaling of the relevant energy sources

$\frac{\partial m}{\partial x_3}$	$\kappa^2 d$
m_3	d
$[m' \cdot \nu']$	$\ln(\frac{1}{d})\, d^2$
$\mathrm{div}' m'$	d^2
external field	$h'_e\, d$
anisotropy	$Q\, d$
asymmetric Bloch wall	$\kappa^2\, d^2$
Néel wall	$(\ln(\frac{1}{\kappa^2 d}))^{-1}\, d^2$
vortex	$\ln(\frac{1}{\kappa\, d})\, \kappa^2\, d^3$

field strengths, the annular regions of field penetration have merged, and the region of field expulsion is no longer connected. Starting from the same energy-minimizing charge distribution, (7,8) can be solved to give either the pattern of Fig. 4 or the one observed in the thinner samples, Fig. 5. Thus, the energies associated with the two configurations differ only by higher order terms. In the thinner samples, however, the Néel character of the walls leads to a repulsive interaction with the edges, and walls and vortex are never really expelled from the sample (at least up to $H = 1.5$).

Comparing the two types of observed behavior, one is led to conclude that the micromagnetic origin of the hysteretic response of the thicker sample seems to lie in some *small* differences. These differences are small in energy, because they are due to the different mechanisms of interaction of walls and vortices with the lateral boundary, and they are very localized in space. Nevertheless, they are at the root of the dramatic differences between the domain patterns shown in Figures 4 and 5, which in turn determine whether or not hysteresis is triggered. The subtle and elusive nature of these effect is, maybe, at the origin of the continuing fascination they exert on the inquisitive mind.

REFERENCES

[1] A. DeSimone, R.V. Kohn, S. Müller, F. Otto and R. Schäfer, Two-dimensional modelling of soft ferromagnetic films, Proc. Roy. Soc. London A, in press (2001).
[2] H.A.M. van den Berg, Self–consistent domain theory in soft–ferromagnetic media. II. Basic domain structures in thin film objects, J. Appl. Phys. **60**, 1104 (1986)
[3] P. Bryant and H. Suhl, Thin-film magnetic patterns in an external field, Appl. Phys. Lett. **54**, 2224 (1989).
[4] R.J Vanderbei, *Linear Programming: Foundations and Extensions* (Kluwer, Boston, 1996).
[5] L.C. Evans *Partial Differential Equations* (American Mathematical Society, Providence, 1998), Section 10.1.
[6] J.A. Sethian, *Level Set Methods* (Cambridge University Press, 1996).

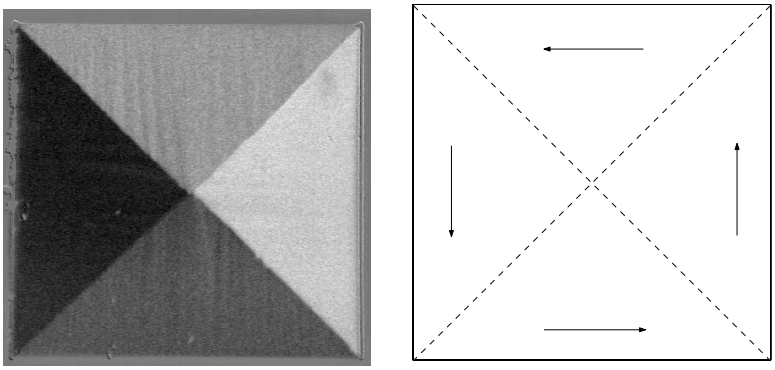

FIGURE 1. AC-demagnetized state. $L = 60$ μm, $D = 230$ nm, $H = 0$.

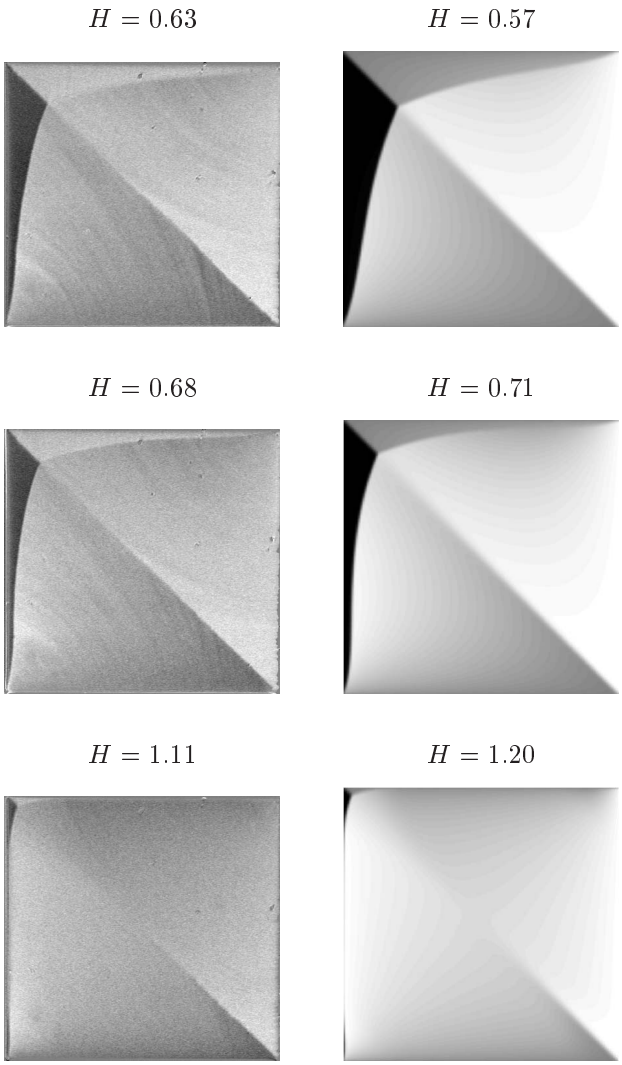

FIGURE 2. Observed domain patterns for $L = 60$ μm, $D = 230$ nm (left column) compared with the predictions of the reduced theory (right column).

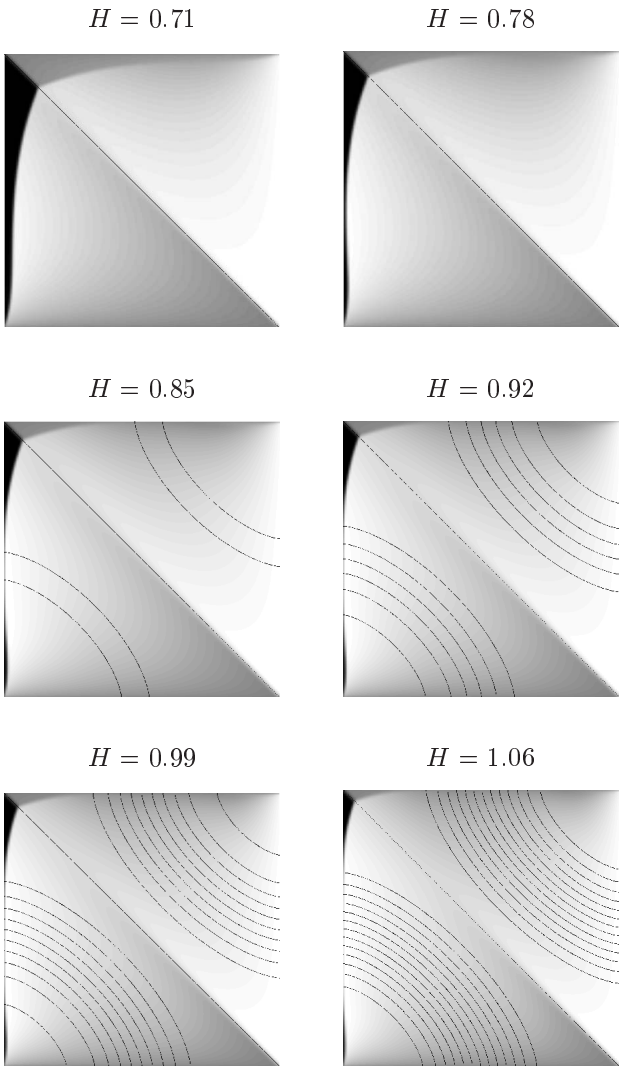

FIGURE 3. The transition between expulsion and penetration regimes: lines are level curves of the potential of the penetrated field.

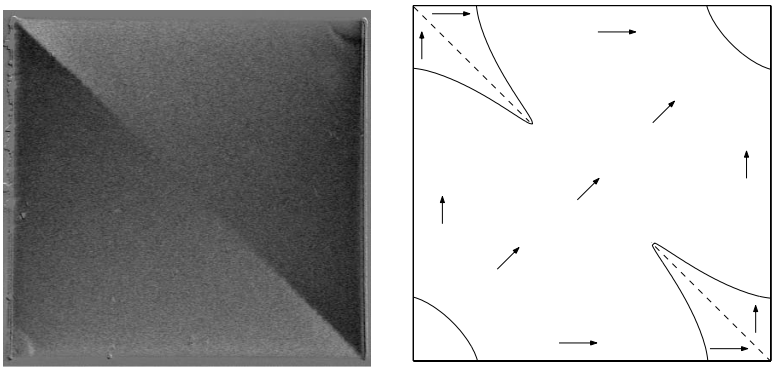

FIGURE 4. Symmetric patterns. $L = 60$ μm, $D = 230$ nm, $H = 1.25$.

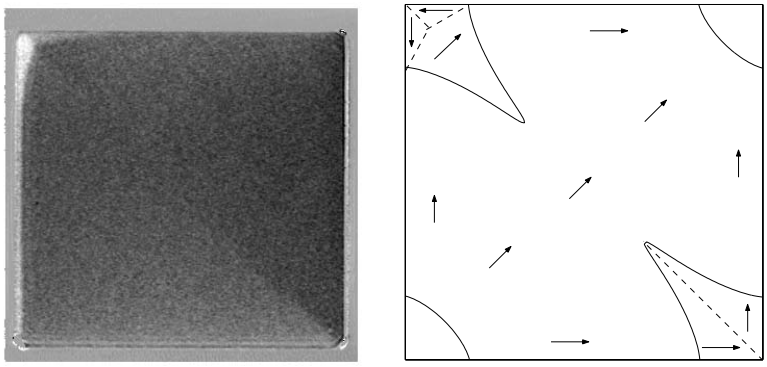

FIGURE 5. Non-symmetric patterns. $L = 30$ μm, $D = 40$ nm, $H = 1.25$.

Antonio DeSimone, Max Planck Institute for Mathematics in the Sciences, Inselstr. 22-26, D-04103 Leipzig, Germany, and Dipartimento di Ingegneria Civile e Ambientale, Politecnico di Bari, I-70126 Bari, Italy
E-mail address: desimone@mis.mpg.de

Robert V. Kohn, Courant Institute of Mathematical Sciences, 251 Mercer Str., New York, NY 10012, U.S.A.
E-mail address: kohn@cims.nyu.edu

Stefan Müller, Max Planck Institute for Mathematics in the Sciences, Inselstr. 22-26, D-04103 Leipzig, Germany
E-mail address: sm@mis.mpg.de

Felix Otto, Institut für Angewandte Mathematik, Universität Bonn, Wegelerstr. 10, D-53115, Bonn, Germany
E-mail address: otto@riemann.iam.uni-bonn.de

Rudolf Schäfer, Institut für Festkörper- und Werkstofforschung, Helmholtzstr. 10, D-01069, Dresden, Germany
E-mail address: r.schaefer@ifw-dresden.de